Development of an improved mathematical model for the dynamic response of a sphere located at a viscoelastic medium interface

This is a post-refereeing final draft. When citing, please refer to the published version: Hasan Koruk (2022), Development of an improved mathematical model for the dynamic response of a sphere located at a viscoelastic medium interface, European Journal of Physics, 43 (2), 025002, DOI: 10.1088/1361-6404/ac4647.
https://doi.org/10.1088/1361-6404/ac4647

Development of an improved mathematical model for the dynamic response of a sphere located at a viscoelastic medium interface

H Koruk[1]
[1]Mechanical Engineering Department, MEF University, 34396 Istanbul, Turkey

Tel.: +902123953654. Email: korukh@mef.edu.tr

Abstract

A comprehensive investigation on the static and dynamic responses of a sphere located at elastic and viscoelastic medium interfaces is performed in this study. First, the mathematical models commonly used for predicting the static displacement of a sphere located at an elastic medium interface are presented and their performances are compared. After that, based on the finite element analyses, an accurate mathematical model to predict the static displacement of a sphere located at an elastic medium interface valid for different Poisson's ratios of the medium and small and large sphere displacements is proposed. Then, an improved mathematical model for the dynamic response of a sphere located at a viscoelastic medium interface is developed. In addition to the Young's modulus of the medium and the radius of the sphere, the model takes into account the density, Poisson's ratio and viscosity of the medium, the mass of the sphere and the radiation damping. The effects of the radiation damping, the Young's modulus, density and viscosity of the medium and the density of the sphere on the dynamic response of the sphere located at a viscoelastic medium interface are explored. The developed model can be used to understand the dynamic responses of spherical objects located at viscoelastic medium interfaces in practical applications. Furthermore, the proposed model is a significant tool for graduate students and researchers in the fields of engineering, materials science and physics to gain insight into the dynamic responses of spheres located at viscoelastic medium interfaces.

Keywords: interface; sphere; large oscillation; modified Hertz model; radiation damping; viscosity; viscoelastic medium.

1. Introduction

There are many applications that spheres are located at medium interfaces [1–8]. The Hertzian contact is referred to the frictionless contact between two bodies; the spherical contact is a special case of the Hertz contact between two spheres or between a sphere and the surface of a half space [6,9]. Some modified Hertz models have been proposed for more accurate estimates for static loading [10–12]. In addition to the Young's modulus of the medium and the radius of the sphere, the effects of the density and viscosity of the medium, the mass of the sphere and the radiation damping can be crucial for dynamic loading. There have been some studies on the investigation of the small [13] and nonlinear [14] oscillations of a sphere on an elastic half space. A mathematical model has been proposed to predict the dynamic response of a sphere located at a medium interface by taking into account the

damping of the oscillations of the sphere due to the radiation of shear waves [15]. The model in [15] has been evaluated using the responses of the bubble and the sphere in a medium [16] and the bubble located at a medium interface [17,18], and it has been concluded that the model produces reasonable results [19]. Furthermore, a finite element model for the sphere located at an elastic interface has been developed and an improved analytical model for the sphere located at an elastic interface has been suggested when the Poisson's ratio of the medium is $\nu = 0.45$ [20]. The equation of motion for this model is given by [20]:

$$\frac{1}{3}\pi R^3\left(4\rho_s + \frac{u_0}{R}\rho\right)\ddot{u} + \frac{1}{2}\left(\beta + \frac{u_0}{R}\right)\left(\sqrt{\frac{\rho}{G}}R\right)\left(1 - \alpha\frac{u_0}{R}\right)1.5 f_0^{1/3}\left(\frac{4E^*\sqrt{R}}{3}\right)^{2/3}\dot{u} + \left(1 - \alpha\frac{u_0}{R}\right)1.5\left(\frac{4E^*\sqrt{R}}{3}\right)^{2/3} f_0^{1/3} u = \left[1 + 0.5\left(1 - \alpha\frac{u_0}{R}\right)\right] f_0 \quad (1)$$

where R and ρ_s are the radius and density of the sphere, ρ and G are the density and shear modulus of the medium material, f_0 and τ are the amplitude and duration of the applied rectangular pulse, $\alpha = 0.1$, $\beta = 0.5$, $u_0 = \left(\frac{3f_0}{4E^*\sqrt{R}}\right)^{2/3}$ is the static displacement of the sphere, E^* is the reduced Young's modulus computed as $1/E^* = \left(1 - \nu_{\text{sphere}}^2\right)/E_{\text{sphere}} + (1 - \nu^2)/E$ where E and ν are the Young's modulus and Poison's ratio of the medium material and E_{sphere} and ν_{sphere} are the Young's modulus and Poison's ratio of the sphere material, respectively, and u, $\dot{u}$, and $\ddot{u}$ are the displacement, velocity and acceleration of the sphere at any time t.

It should be noted that there are different models such as the Kelvin-Voigt, Maxwell and standard linear solid models for modelling viscoelastic materials [21–23]. It was shown that the Kelvin-Voigt model can properly simulate viscoelastic materials, e.g., it can properly simulate the creep behaviour [16,24]. In some mathematical models, the medium under investigation is assumed to be infinite and these models can produce reasonable results for structures with finite dimensions [16,18,24–26]. For example, the dynamic response of a rigid sphere with a radius of 0.75 mm located inside a cylindrical finite medium (gelation and rubber phantoms) with a radius of 30 mm and height of 80 mm predicted by the finite element model was shown to be very close to the response predicted by the analytical model based on the infinite medium assumption [25]. The measured dynamic response of a magnetic sphere with a radius of 1 mm located inside a medium (gelation phantom) of cylindrical shape with a diameter of 30 mm and a volume of 25 ml was shown to be very close to the response predicted by the analytical model based on the infinite medium assumption [26]. Similarly, the measured dynamic response of a microbubble with a radius of 1.5-2.0 mm located at the interface of a finite medium (hydrogel) with a width of 15 mm, height of 15 mm and depth of 10 mm was shown to be close to the response predicted by the analytical model based on the infinite medium assumption [24]. The medium can be assumed to be infinite when the size of the particle interacting with the medium is much less than the size of the medium under investigation. It should be noted that the medium under investigation can be assumed to be semi-infinite in the mathematical models or the finite medium can be directly modelled by applying the appropriate boundary conditions. For the dynamic stability control of

nanocomposite piezoelectric sandwich beams on a foundation, the Kelvin-Voigt was considered for the sandwich structure and the Kerr viscoelastic foundation was enhanced [23]. The effects of various kinds of viscoelastic foundations including visco-Winkler, visco-Pasternak and visco-Kerr on the instability region of the system were illustrated [23]. For the dynamic buckling analysis of carbon nanocones, the structural damping influences were studied according to the Kelvin-Voigt model, while the medium around the carbon nanocones was assumed by the model of visco-Pasternak [27]. For the vibration analysis of nanoplates resting on a medium, the material properties of the nanoplate were assumed to be orthotropic and viscoelastic and the viscoelastic medium was modelled as the Kelvin-Voigt foundation [28]. The reader may refer to the recent studies [29–32] for the use of viscoelastic models to model the medium under investigation and different methods for simulating the surrounding medium. It should be noted that the elastic solutions to the steady state boundary-value problems can be transformed into the viscoelastic solutions for the identical boundary conditions by using the so-called elastic-viscoelastic correspondence principle [33–38]. There are viscoelastic mixed boundary value problems where the regions, over which different types of boundary conditions are given, vary with time; a particular example is the indentation problem [34,38]. It is stated that the validity of the classical correspondence principle is restricted to problems where the prescribed boundary conditions are time-invariant [35,37,38].

A comprehensive investigation on the static and dynamic responses of a sphere located at elastic and viscoelastic medium interfaces is performed in this study. The contributions of this study are listed as follows: (i) The mathematical models commonly used for predicting the static displacement of the sphere located at an elastic medium interface are presented and their performances are compared. (ii) Based on the finite element analyses, an accurate mathematical model to predict the static displacement of the sphere located at an elastic medium interface valid for different Poisson's ratios of the medium and small and large sphere displacements is proposed. (iii) The model for the sphere located at an elastic medium interface [20] is extended to develop an improved mathematical model for the dynamic response of the sphere located at a viscoelastic medium interface (see figure 1). In addition to the elastic properties of the medium and the radius of the sphere, the model takes into account the density, Poisson's ratio and viscosity of the medium, the mass of the sphere and the radiation damping and it is valid for small and large sphere displacements. The effects of the radiation damping, the Young's modulus, density, and viscosity of the medium and the density of the sphere on the dynamic response of the sphere located at a viscoelastic medium interface are explored.

The developed model can be used to understand the dynamic responses of spherical objects located at viscoelastic medium interfaces in practical applications. Furthermore, the proposed model is a significant tool for graduate students and researchers in the fields of engineering, materials science and physics to gain insight into the dynamic responses of spheres located at viscoelastic medium interfaces. The students and researchers clearly see the performances of different mathematical models commonly used for predicting the static displacement of the sphere located at an elastic medium interface. Using the procedure in this

study, the students and researchers can understand, based on the need, how to convert the equation of motion in the time domain to the frequency domain, how to include the viscosity of the medium in the model, and how to solve the complicated equation of motion using the inverse Fourier transform. The procedure followed in this study is illustrated in figure 2.

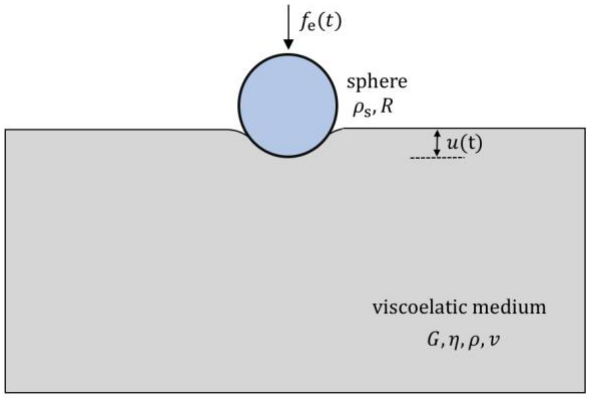

Figure 1. The schematic picture for the sphere located at a viscoelastic medium interface.

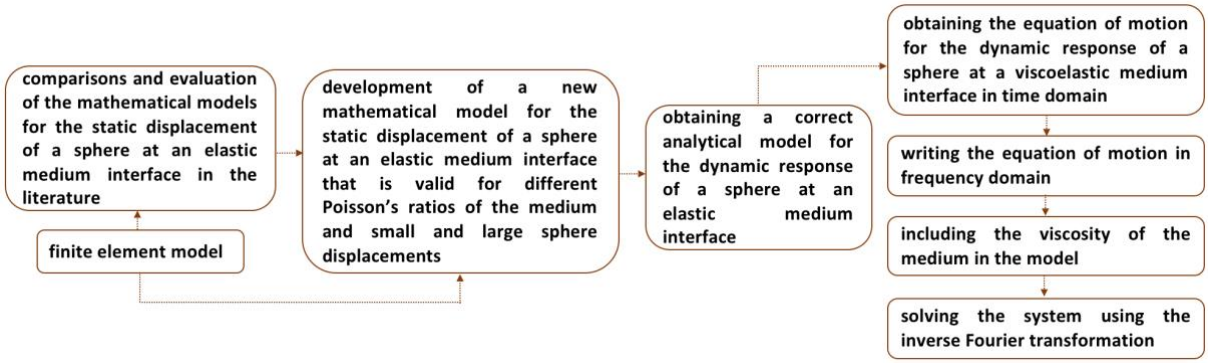

Figure 2. The procedure followed in this study.

2. Mathematical models for the sphere located at an elastic medium interface exposed to a static force

2.1 Hertz model (Model 1)

It was shown that the Hertz theory significantly underestimates the contact radius and overestimates the maximum contact pressure as the ratio of the indentation depth to indenter radius exceeds 0.1, hence the Hertz model is valid when the ratio of the indentation depth to indenter radius is less than 0.1 [39]. For the Hertz model, the relationships between the applied force (f_0), the contact depth (u_a), the contact radius (a) and the deformation depth (u_0) are as follows [7,15]:

$$f_0 = \frac{4E\sqrt{R}}{3(1-v^2)} u_0^{3/2} \tag{2a}$$

$$u_a = \frac{u_0}{2} \tag{2b}$$

$$a = \sqrt{R u_0} \tag{2c}$$

2.2 Sneddon model (Model 2)

For some soft materials that exhibit large elastic deformations, including the rubber-like materials, gels and biological materials, the large indentation is needed to minimize the measurement noise [11]. The accurate solution regarding the interaction of a rigid sphere and a soft elastic half space is given by the Sneddon model [10,40]:

$$f_0 = \frac{E}{2(1-\nu^2)}\left[(a^2+R^2)\ln\left(\frac{R+a}{R-a}\right) - 2aR\right] \tag{3a}$$

$$u_0 = \frac{1}{2}a\ln\left(\frac{R+a}{R-a}\right) \tag{3b}$$

For large indentation depths, a series solution for the load-displacement relation can be obtained using the Sneddon model. An approximate Sneddon model is presented in the next section.

2.3 Approximate Sneddon model (Model 3)

The expressions given above (Eq. 3) do not provide a direct relation between the applied force and the deformation depth. Kontomaris and Malamou [7], based on the Sneddon's model, proposed a model that directly relates the applied force to the deformation depth when a rigid sphere is pushed into an elastic half space (regardless of the value of the maximum deformation depth). This approximate Sneddon model is given by:

$$f_0 = \frac{4E\sqrt{R}}{3(1-\nu^2)}u_0^{3/2}\left[c_1 + \sum_{k=2}^{n}\frac{3}{2k}c_k R^{(3/2-k)}u_0^{k-3/2}\right] \tag{4}$$

For $n = 6$, $c_1 = 1.01$, $c_2 = -0.07303$, $c_3 = -0.1357$, $c_4 = 0.03598$, $c_5 = -0.0042024$, and $c_6 = 0.0001653$.

2.4 Modified Hertz model (Model 4)

Guo et al. [11] proposed a modified Hertz model inspired by numerical simulations to predict the contact response of a linearly elastic half-space under finite (large) spherical indentations. In this model, the relation between the applied force and the contact radius is given by:

$$f_0 = \frac{2\pi}{3}p_0 a^2 \tag{5a}$$

where

$$p_0 = \frac{2E}{\pi(1-\nu^2)}\frac{u_0}{a}\frac{\beta_1(1+\beta_1)}{\ln(1+\beta_1)} \tag{5b}$$

$$\beta_1 = -\frac{u_r(a)}{a} \tag{5c}$$

$$u_r(a) = -\frac{2(1-2\nu)}{3\pi(1-\nu)}\left(u_0 - \frac{1}{4R}u_0^2\right) \tag{5d}$$

$$a = \sqrt{Ru_0 - u_0^2/4} \tag{5e}$$

Using the equations above, the following relation can be obtained:

$$f_0 = \frac{2\pi}{3}\frac{2E}{\pi(1-\nu^2)}u_0\frac{\beta_1(1+\beta_1)}{\ln(1+\beta_1)}a \tag{6a}$$

or

$$f_0 = \frac{2\pi}{3}\frac{2E}{\pi(1-\nu^2)}u_0\frac{\frac{2(1-2\nu)}{3\pi(1-\nu)}\left(u_0-\frac{1}{4R}u_0^2\right)(1+\beta_1)}{\ln(1+\beta_1)} \tag{6b}$$

Hence, the relation between the applied force and indentation depth for the modified Hertz model is obtained as follows:

$$f_0 = \frac{2\pi}{3}\frac{2E}{\pi(1-\nu^2)}u_0\frac{\frac{2(1-2\nu)}{3\pi(1-\nu)}\left(u_0-\frac{1}{4R}u_0^2\right)\left[1+\frac{\frac{2(1-2\nu)}{3\pi(1-\nu)}\left(u_0-\frac{1}{4R}u_0^2\right)}{\sqrt{Ru_0-u_0^2/4}}\right]}{\ln\left[1+\frac{\frac{2(1-2\nu)}{3\pi(1-\nu)}\left(u_0-\frac{1}{4R}u_0^2\right)}{\sqrt{Ru_0-u_0^2/4}}\right]} \tag{7}$$

It is seen that the model proposed by Guo et al. [11] is quite complicated and explicit solution for sphere displacement seems impossible.

2.5 Hertz model corrected for sample thickness (Model 5)

The following thickness-corrected Hertz model is suggested for a sample with finite thickness *h* [12]:

$$f_0 = \frac{4E}{3(1-\nu^2)}\sqrt{R}u_0^{3/2}\left[1-\frac{2\alpha_0}{\pi}\chi+\frac{4\alpha_0^2}{\pi^2}\chi^2-\frac{8}{\pi^3}\left(\alpha_0^3+\frac{4\pi^2}{15}\beta_0\right)\chi^3+\frac{16\alpha_0}{\pi^4}\left(\alpha_0^3+\frac{3\pi^2}{5}\beta_0\right)\chi^4\right] \tag{8a}$$

where

$$\chi = \frac{\sqrt{Ru_0}}{h} \tag{8b}$$

Here, α_0 and β_0 are given as:

$$\alpha_0 = -0.347\frac{3-2\nu}{1-\nu} \tag{8c}$$

$$\beta_0 = 0.056\frac{5-2\nu}{1-\nu} \tag{8d}$$

when the sample is not bonded to the substrate. These coefficients are given as:

$$\alpha_0 = -\frac{1.2876-1.4678\nu+1.3442\nu^2}{1-\nu} \tag{8e}$$

$$\beta_0 = \frac{0.6387-1.0277\nu+1.5164\nu^2}{1-\nu} \tag{8f}$$

when the sample is bonded to the substrate.

2.6 Hertz model corrected for sphere displacement (Model 6)

Koruk [20] proposed an improved dynamic Hertz model based on finite element analyses for small and large sphere displacements and a Poisson's ratio of $\nu = 0.45$. For a static applied force where the contact between the sphere and medium is continuous, the model can be written as:

$$f_0 = \left[\frac{1-0.1\frac{u_0}{R}}{1+0.5\left(1-0.1\frac{u_0}{R}\right)}\right]^{3/2}\frac{4E\sqrt{R}}{3(1-\nu^2)}u_0^{3/2} \quad \text{for } \nu = 0.45 \tag{9}$$

2.7 Hertz model corrected for sphere displacement and the Poisson's ratio of the medium (Model 7)

As stated before, the model above (Eq. 9) is proposed for a Poisson's ratio of the medium of $\nu = 0.45$ [20]. However, the finite element analysis results performed for different

values of v show that the difference between the model in [20] and the finite element model can be considerable. In this study, a model is proposed to include the correction for the Poisson's ratio of the medium. It was shown in [20] that the correction factor 0.1 (i.e., $0.1u_0/R$) produces very accurate results for v = 0.45. In this current study, the force values predicted by the model in [20] for different correction factors (e.g., -0.1, -0.05, 0.1, 0.0, 0.05, 0.1) were compared with the results predicted by the finite element model. It was seen that the force values predicted by the analytical model and the finite element model for different values of u_0/R match well when the correction factor is around -0.1, -0.05, 0.0, 0.05, 0.1 and 0.14 when v = 0.25, 0.30, 0.35, 0.40, 0.45 and 0.49, respectively (the results are shown in Section 2.9). This shows that the correction factor is a function of v and can be written as $v - 0.35$. It means that the correct force for a specific sphere displacement should decrease as the Poisson's ratio of the medium material increases. Hence, the model in [20] is updated as follows:

$$f_0 = \left\{\frac{1-(v-0.35)\frac{u_0}{R}}{1+0.5\left[1-(v-0.35)\frac{u_0}{R}\right]}\right\}^{3/2} \frac{4E\sqrt{R}}{3(1-v^2)}u_0^{3/2} \quad (10)$$

All the seven models including the new model presented in this paper (Model 7) are compared and evaluated in Section 2.9.

2.8 Finite element model

A finite element model for the sphere at an elastic interface is used to assess the performance of the mathematical models. The finite element model of the system is developed using axisymmetric quadrilateral finite elements in the Abaqus software (Dassault Systèmes, France). For the finite element model of the sphere at a medium interface, the elastic medium is modelled using linear quadrilateral axisymmetric reduced integration elements of type CAX4R and the sphere is modelled using linear line elements of type RAX2. Here, a cylindrical medium of h = 100 mm height and r = 100 mm radius is modelled using 130235 CAX4R elements and the sphere is modelled using 29 RAX2 elements. The medium is partitioned to able to use fine mesh around the sphere and coarser mesh far from the sphere. The sphere displacement in horizontal direction is restricted and the contact between the sphere and medium is frictionless. The horizontal motion for the left edge of the medium and the vertical motion for the bottom edge of the medium are restricted (figure 3). It should be noted that a second finite element model with a cylindrical medium of h = 50 mm height and r = 50 mm radius (55000 CAX4R and 29 RAX2 elements) is used to check the results. Although the results of the cylindrical medium of h = 100 mm and r = 100 mm are presented in the sections below, the comparisons showed that the displacements of the sphere in the time range of interest for both finite element models are almost the same (the numerical difference between the displacements predicted by two models is less than 0.2%). For the comparisons of the analytical and finite element models below, the same discrete displacement vector (when predicting the force as a function of sphere displacement) and the same discrete time vector (when predicting the sphere displacement as a function of time) are used for the analytical and finite element models to eliminate the errors due to discretization in the following sections.

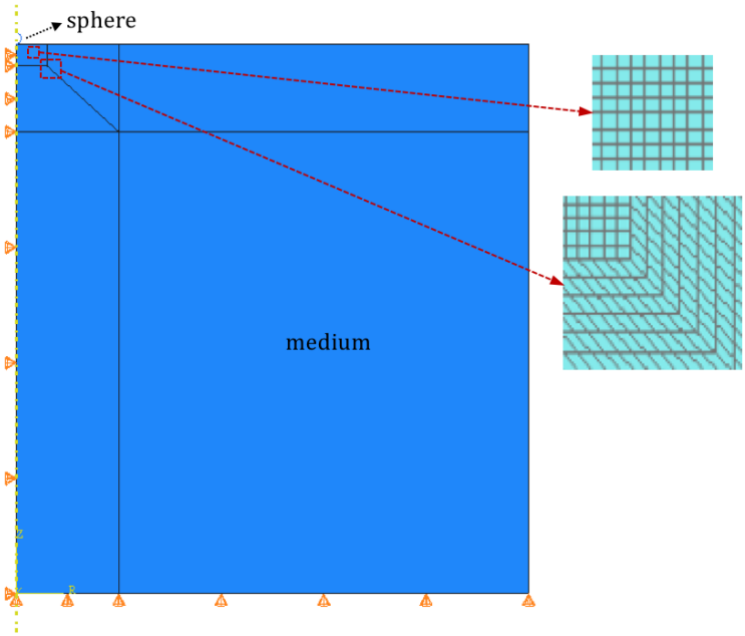

Figure 3. The partitioned medium for the use fine mesh around the sphere and coarser mesh far from the sphere and the boundary conditions.

2.9 Comparisons and evaluation

The force predicted by all seven models and the finite element model presented above are plotted as a function of dimensionless sphere displacement (u_0/R) in figure 4 ($E = 10000$ Pa, $\nu = 0.40$ and $R = 0.5$ mm). In order to clearly see the performances of the models, the differences between the force predicted by the seven models and the finite element model for different values of the Poisson's ratio of the medium are plotted in figure 5 ($E = 10000$ Pa and $R = 0.5$ mm). It is seen that the performances of the models are dependent on the Poisson's ratio of the medium. The differences between the predicted force by the Hertz model corrected for sphere displacement and the Poisson's ratio of the medium (Model 7) and the finite element model are minimum for all dimensionless sphere displacements and Poisson's ratios of the medium. The error generally increases as dimensionless sphere displacement increases for all models except the model proposed in this study (Model 7). The results predicted by the Hertz model corrected for sphere displacement (Model 6) and by the Hertz model corrected for sphere displacement and the Poisson's ratio of the medium (Model 7) are the same for $\nu = 0.45$ as expected, because Model 6 is proposed for $\nu = 0.45$. The results of the Sneddon Model (Model 2) and the Hertz model corrected for sphere displacement (Model 6) are very close to each other. The results predicted by the Sneddon model (Model 2) and the approximate Sneddon model (Model 3) are close to each other, though the Sneddon model produces slightly lower errors. The results predicted by the Hertz model (Model 1) and the Hertz model corrected for medium thickness (Model 5) are almost the same, because the thickness of the medium compared to sphere radius is quite high (i.e., h/R = 100/0.5 = 200). It is seen that Model 4 always overestimates the force, while Models 2, 3 and 6 always underestimate the force.

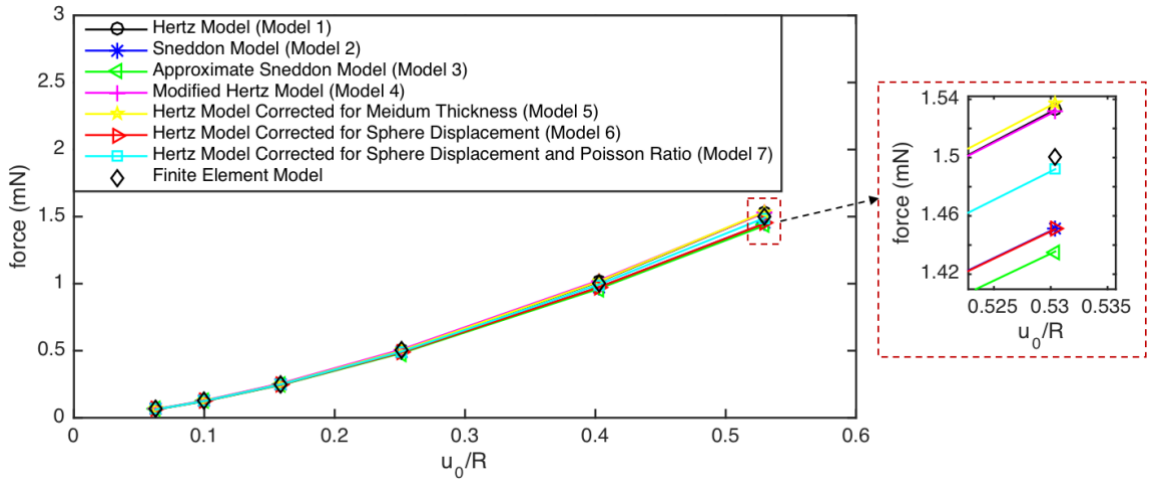

Figure 4. The force predicted by all seven models and the finite element model as a function of dimensionless sphere displacement ($E = 10000$ Pa, $\nu = 0.40$ and $R = 0.5$ mm).

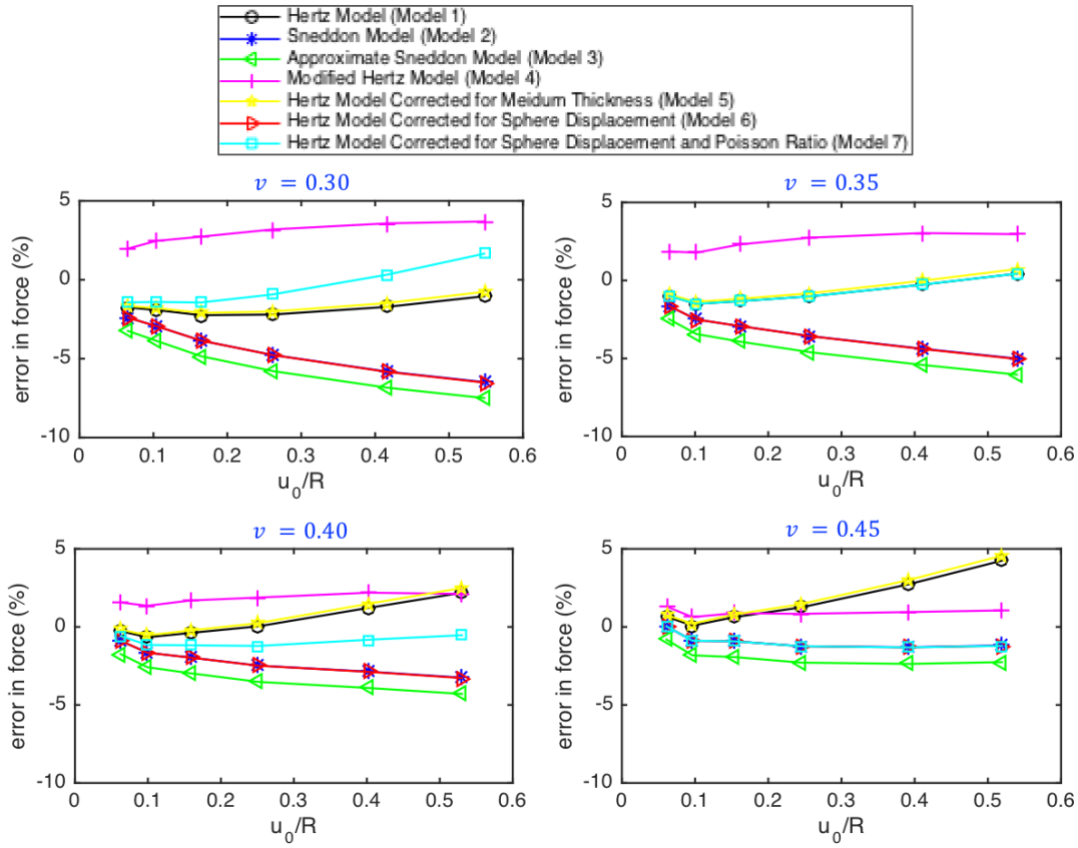

Figure 5. The differences between the force predicted by the seven models and the finite element model for different values of the Poisson's ratio of the medium as a function of dimensionless sphere displacement ($E = 10000$ Pa and $R = 0.5$ mm).

The average absolute errors in the predicted force for dimensionless sphere displacement from 0.065 to 0.55 as a function of the Poisson's ratio of the medium are plotted in figure 6 ($E = 10000$ Pa and $R = 0.5$ mm). It is seen that the Hertz model (Model 1) and the Hertz model corrected for medium thickness (Model 5) work best when $\nu = 0.35 - 0.40$.

The error in the force predicted by the Sneddon model (Model 2), approximate Sneddon model (Model 3), modified Hertz model (Model 4) and the Hertz model corrected for sphere displacement (Model 6) decreases as the Poisson's ratio of the medium increases; these model work best at $\nu = 0.49$. On the other hand, the error is small for all Poison's ratios of the medium for the Hertz model corrected for sphere displacement and the Poisson's ratio of the medium (Model 7, the model proposed in this study). Overall, the results show that, among the given seven models, the model proposed in this study (Model 7) produces minimum errors for all dimensionless sphere displacements and Poisson's ratios of the medium. The error in the force predicted by Model 7 is around 1%. It should be noted that, for an applied force, the error in the induced displacement is approximately 70% less than the error in the predicted force. That is, the error produced by Model 7 in the induced sphere displacement is less than 0.7% for practical Poisson's ratios of the medium (i.e., $\nu = 0.30 - 0.45$) and small and large (i.e., $u_0/R = 0.6$) sphere displacements.

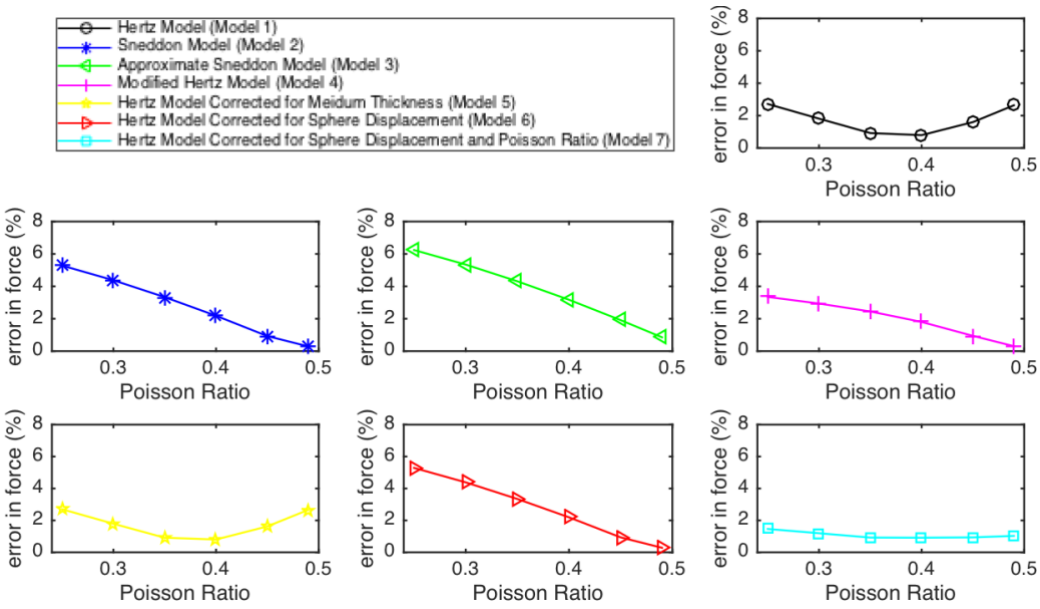

Figure 6. The average absolute errors in the predicted force for dimensionless sphere displacement from 0.065 to 0.55 as a function of the Poisson's ratio of the medium ($E = 10000$ Pa and $R = 0.5$ mm).

3. Updating the mathematical model for the sphere located at an elastic medium interface exposed to a dynamic force

Based on a finite element model for the sphere located at an elastic interface, an improved analytical model for the sphere located at an elastic interface exposed to a dynamic force has been suggested [20]. However, this model has been corrected for the Poisson's ratio of the medium of $\nu = 0.45$ and the correction factor has been determined to be $\left(1 - \alpha \frac{u_0}{R}\right)$ where $\alpha = 0.1$ [20]. In this current study, based on a huge number of finite element analyses, a mathematical model for all practical Poisson's ratios of the medium is suggested. In this model, the correction factor is given by $\left(1 - \alpha \frac{u_0}{R}\right)$ where $\alpha = \nu - 0.35$ (Model 7). Hence, by

replacing $\left(1-0.1\frac{u_0}{R}\right)$ in Eqs. 7, 9, 11, 12, 14, 15 and 17 in Ref. [20] with $\left[1-(v-0.35)\frac{u_0}{R}\right]$, an analytical model for the sphere located at an elastic interface (no medium viscosity) exposed to a dynamic force that is valid for all practical Poisson's ratios of the medium can be obtained. The modified equations are not regenerated here for brevity.

The displacements of the sphere located at an elastic medium interface for different forces and Poisson's ratios of the medium precited by the analytical model in [20], the updated model proposed in this study and the finite element model are shown in figures 7-8 ($E = 10000$ Pa, $\rho = 1000$ kg/m^3, $R = 0.5$ mm and ρ_s = 9000 kg/m^3). It is seen that the results predicted by the updated analytical model and the finite element model are very close to each other. For any applied force and Poisson's ratio of the medium, the amplitudes and period of oscillations and the steady-state displacements predicted by the updated model are very close to the ones predicted by the finite element model. As the analytical model in [20] has been corrected for $v = 0.45$, this model produces accurate results when the Poisson's ratio of the medium is close to $v = 0.45$. Although the results not presented here for brevity, it is seen that the results predicted by the analytical model in [20] and the updated model proposed in this study are exactly the same for $v = 0.45$ and the differences between the analytical model in [20] and the finite element model (or the updated analytical model) increase when the Poisson's ratio of the medium gets far from $v = 0.45$.

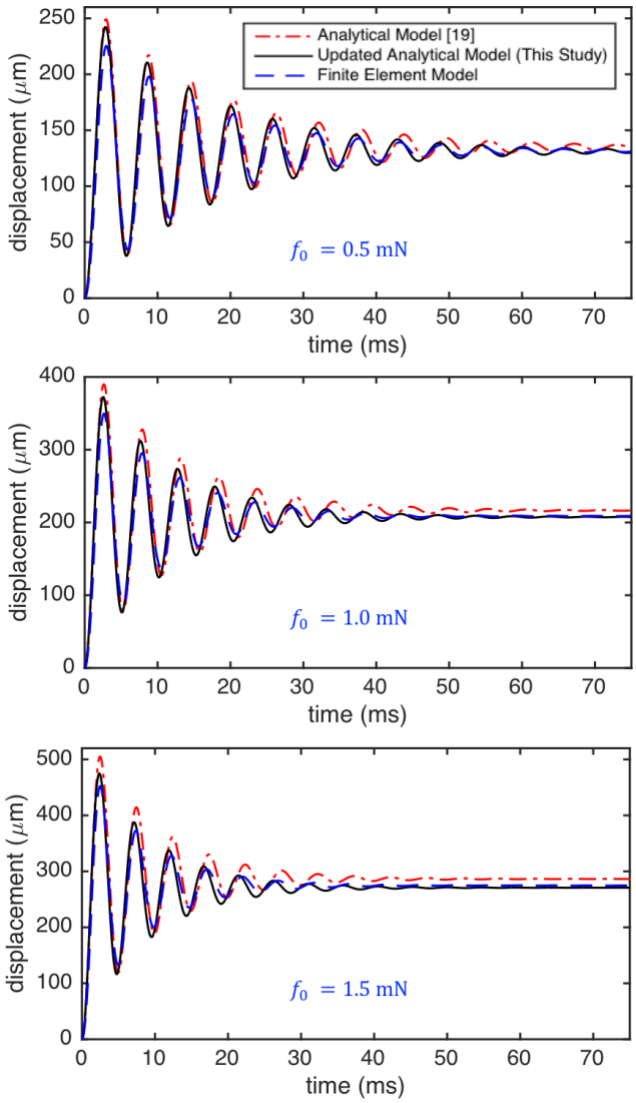

Figure 7. The displacements of the sphere located at an elastic medium interface for different forces precited by the analytical model in [20], the updated model proposed in this study and the finite element model ($E = 10000$ Pa, $\rho = 1000$ kg/m^3, $R = 0.5$ mm, ρ_s = 9000 kg/m^3 and $v = 0.30$).

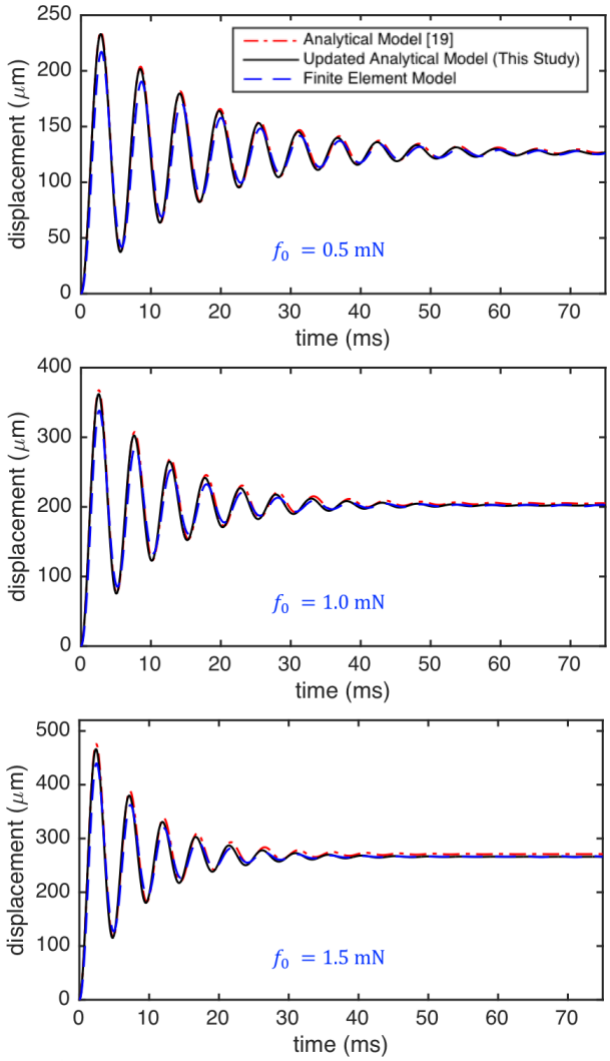

Figure 8. The displacements of the sphere located at an elastic medium interface for different forces precited by the analytical model in [20], the updated model proposed in this study and the finite element model ($E = 10000$ Pa, $\rho = 1000$ kg/m^3, $R = 0.5$ mm, ρ_s = 9000 kg/m^3 and $v = 0.40$).

4. Development of an improved mathematical model for the sphere located at a viscoelastic medium interface exposed to a dynamic force

The hysteretic or structural damping model or rheological models such as the Maxwell, Kelvin-Voigt and standard linear solid models where springs and dampers are arranged in series and/or parallel can be used to include damping for viscoelastic materials in order to determine their stress or strain interactions [16,41,42]. For example, in the Kelvin-Voigt model, the stress is given by $G\varepsilon + \eta\dot{\varepsilon}$ in the time domain, being $(G - j\eta\omega)\epsilon$ in the frequency domain. It was shown that the Kelvin-Voigt model can properly simulate viscoelastic materials, e.g., it can properly simulate the creep behaviour [16,24]. Therefore, we used the Kelvin-Voigt model in this study. It should be noted that the results presented later in this section show that the sphere displacement (or tissue deformation) increases when the force is applied and it decreases in time when the force is removed as expected. The use of different models for the medium including the Maxwell and standard linear solid models [21–

23] as well as the experimental investigation will be considered in our future studies. Here, it is assumed that there is no sphere displacement in horizontal direction and the contact between the sphere and medium is frictionless and continuous. The medium under investigation is assumed to be infinite in this study. However, the model can be modified for a sample resting on a foundation in future. For example, the structural damping of the sample can be simulated by the Kelvin-Voigt model, while the foundation can be simulated by the visco-Kerr, visco-Winkler or visco-Pasternak model [23]. It should be remembered that a linear viscoelastic model (i.e., Kelvin-Voigt) for medium is used and the plastic deformation is not considered in this study. As the analytical solution with viscosity component is not possible, the equation of motion for the sphere located at an elastic medium interface in the time domain (i.e., Eq. 1) can be first written in the frequency domain. Then, the effect of the viscosity of the medium (η) is taken into account by replacing G with $(G - j\omega\eta)$. It should be noted the Fourier transform of a rectangular pulse with the amplitude of f_0 and the duration of τ is $-\frac{jf_0}{\omega}\left(e^{j\omega\tau} - 1\right)$. Overall, (i) the model correctly estimating the force required for a specific sphere displacement that is valid different v and u_0/R values (Model 7) is used for the model to predict the dynamic response of a sphere at a viscoelastic medium interface. (ii) The effect of the viscosity of the medium is taken into account by using the Kelvin-Voigt model, i.e., by replacing G with $(G - j\omega\eta)$. Hence, by replacing $0.1\frac{u_0}{R}$ with $(v - 0.35)\frac{u_0}{R}$ and G with $(G - j\omega\eta)$ in equation (1), we obtain the equation of motion of the sphere located at a viscoelastic medium interface as:

$$\frac{1}{3}\pi R^3\left(4\rho_s + \frac{u_0}{R}\rho\right)(-\omega^2 U) + \frac{1}{2}\left(\beta + \frac{u_0}{R}\right)\left(\sqrt{\frac{\rho}{G - j\omega\eta}}R\right)\left[1 - (v - 0.35)\frac{u_0}{R}\right]1.5f_0^{1/3}\left(\frac{4\tilde{E}^*\sqrt{R}}{3}\right)^{2/3}(-j\omega U) + \left[1 - (v - 0.35)\frac{u_0}{R}\right]1.5\left(\frac{4\tilde{E}^*\sqrt{R}}{3}\right)^{2/3} f_0^{1/3} U = \left\{1 + 0.5\left[1 - (v - 0.35)\frac{u_0}{R}\right]\right\}\left[-\frac{jf_0}{\omega}\left(e^{j\omega\tau} - 1\right)\right] \quad (11)$$

where $\tilde{E}^* = 2(G - j\omega\eta)(1 + \nu)/(1 - \nu^2)$ for a homogeneous isotropic material and a non-deformable sphere. It should be noted that, by setting $\eta = 0$ in the model of the sphere located at the viscoelastic medium interface in Eq. (11), we obtain the Fourier transform of the model for the sphere located at the elastic medium interface in Eq. (1). Hence, the dynamic response of the sphere located at a viscoelastic medium interface in the frequency domain is obtained as follows:

$$U = \frac{\left\{1+0.5\left[1-(v-0.35)\frac{u_0}{R}\right]\right\}\left[-\frac{jf_0}{\omega}\left(e^{j\omega\tau}-1\right)\right]}{\frac{1}{3}\pi R^3\left(4\rho_s+\frac{u_0}{R}\rho\right)(-\omega^2)+\left[\frac{1}{2}\left(\beta+\frac{u_0}{R}\right)\left(\sqrt{\frac{\rho}{G-j\omega\eta}}R\right)(-j\omega)+1\right]\left[1-(v-0.35)\frac{u_0}{R}\right]1.5f_0^{1/3}\left(\frac{4\tilde{E}^*\sqrt{R}}{3}\right)^{2/3}} \quad (12)$$

The time-domain response of the sphere located at a viscoelastic interface can be found by the inverse Fourier transform as:

$$u(t)=\frac{1}{2\pi}\int_{-\infty}^{\infty}\frac{\left\{1+0.5\left[1-(\nu-0.35)\frac{u_0}{R}\right]\right\}\left[-\frac{jf_0}{\omega}\left(e^{j\omega\tau}-1\right)\right]e^{-j\omega t}}{\frac{1}{3}\pi R^3\left(4\rho_s+\frac{u_0}{R}\rho\right)(-\omega^2)+\left[\frac{1}{2}\left(\beta+\frac{u_0}{R}\right)\left(\sqrt{\frac{\rho}{G-j\omega\eta}}R\right)(-j\omega)+1\right]\left[1-(\nu-0.35)\frac{u_0}{R}\right]1.5f_0^{1/3}\left(\frac{4\tilde{E}^*\sqrt{R}}{3}\right)^{2/3}}\,\mathrm{d}\omega \tag{13}$$

It should be remembered that $\beta = 0.5$. Here, the excitation duration τ is divided into N (e.g., 2000) points and the calculations are repeated over the entire time period of interest using the Matlab software (Mathworks, Natick, MA).

The displacements of the sphere located at a viscoelastic elastic medium interface are shown in figure 9 ($f_0 = 1$ mN, $E = 10000$ Pa, $\rho = 1000$ kg/m^3, $\nu = 0.40$, $\eta = 0.5$ Pa s, $R = 0.5$ mm and $\rho_s = 9000$ kg/m^3). The results without and with the radiation damping are also included in figure 9. It is seen that the damping due to the oscillations of the sphere due to the radiation of shear waves is considerable and the amplitudes of oscillations are further decreased with the viscosity of the medium. The energy at a time $t = t_2$ can be written in terms of the energy components at a former time $t = t_1$ using $T_2 + S_2 = T_1 + S_1 - E_d$ where T, S and E_d show the kinetic, strain and dissipated energy components, respectively. At the time points where the displacement is maximum (i.e., peaks), the kinetic energy is zero. Hence, we can write $E_d = S_1 - S_2 = \frac{1}{2}k(u_1^2 - u_2^2)$ where u_1 and u_2 represent the displacements at two different peaks. Using the information for the first two peaks in figure 9 (i.e., using the peaks at $t = 2.5$ and 7.6 s), the dissipated energy is calculated to be $E_d = 0$, 1.08 and 1.22 micro Joule/cycle when the radiation damping is ignored, only the radiation damping is considered and both the radiation damping and medium viscosity are considered, respectively. As expected, the dissipated energy is zero for the undamped system and the dissipated energy further increases as the medium viscosity is taken into account.

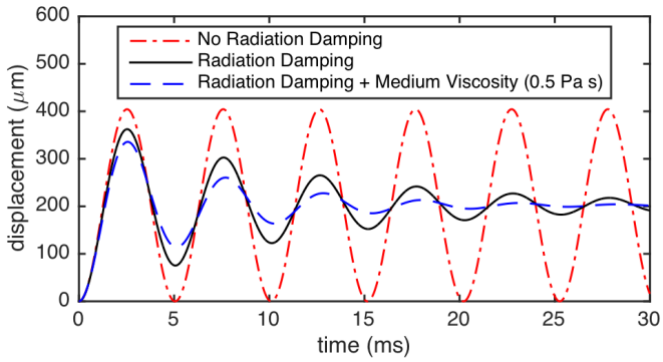

Figure 9. The displacements of the sphere located at a viscoelastic elastic medium interface ($f_0 = 1$ mN, $E = 10000$ Pa, $\rho = 1000$ kg/m^3, $\nu = 0.40$, $\eta = 0.5$ Pa s, $R = 0.5$ mm and $\rho_s = 9000$ kg/m^3).

The displacements of the sphere located at a viscoelastic elastic medium interface for different excitation duration and medium viscosity values are shown in figure 10 ($f_0 = 1$ mN, $E = 10000$ Pa, $\rho = 1000$ kg/m^3, $\nu = 0.35$, $R = 0.5$ mm and $\rho_s = 5000$ kg/m^3). It is seen that the amplitudes of oscillations decrease as medium viscosity increases. There are almost

no oscillations when the medium viscosity is high enough (i.e., $\eta = 4$ Pa s). The system reaches the steady-state after a certain time. For example, for $\tau = 2$ ms, there are no vibrations around the steady-state position, because there is no enough time to set vibrations around this position. On the other hand, the sphere can oscillate around the steady-state position for $\tau = 10$ and 20 ms. It is seen that the time to reach the steady-state decreases as the viscosity of the medium increases. However, the amount of the viscosity of the medium does not change the steady-state displacement.

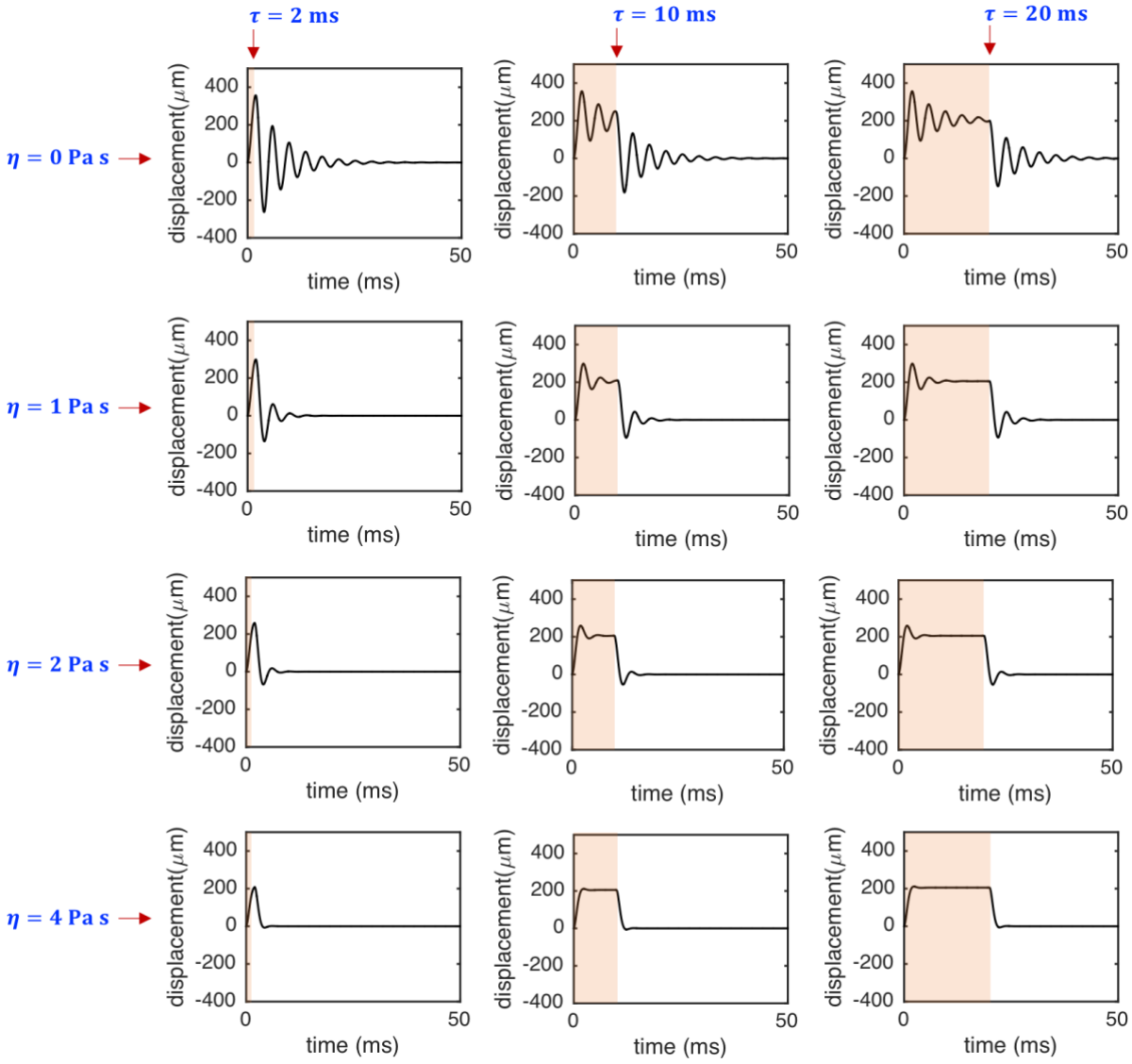

Figure 10. The displacements of the sphere located at a viscoelastic elastic medium interface for different excitation duration and medium viscosity values ($f_0 = 1$ mN, $E = 10000$ Pa, $\rho = 1000$ kg/m^3, $\nu = 0.35$, $R = 0.5$ mm and $\rho_s = 5000$ kg/m^3). The excitation starts at $t = 0$ and the arrow shows the end of the excitation.

The displacements of the sphere located at a viscoelastic elastic medium interface for different Young's moduli and viscosities of the medium are shown in figure 11 ($f_0 = 0.5$ mN, $\rho = 1000$ kg/m^3, $\nu = 0.40$, $R = 0.5$ mm and $\rho_s = 9000$ kg/m^3). The spectrums of the time

domain data are also included in figure 11. The spectrums clearly show the changes in the amplitudes and frequency of oscillations. The amplitudes of oscillations decrease and the frequency of oscillations increases as the Young's modulus of the medium increases as expected. It is clearly seen that the viscosity of the medium has huge effects on the amplitudes of oscillations and the viscosity of the medium should be considered for dynamic loading.

.

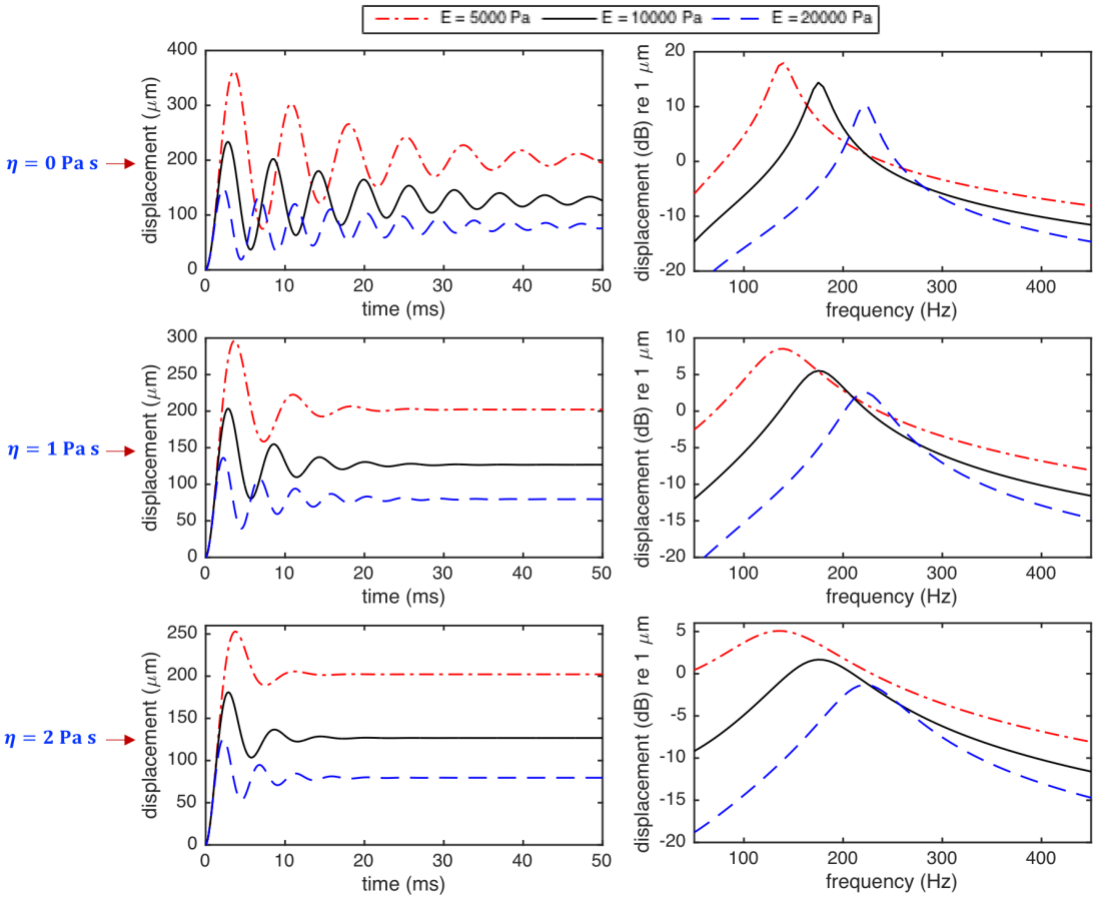

Figure 11. The displacements of the sphere located at a viscoelastic elastic medium interface for different Young's moduli and viscosities of the medium ($f_0 = 0.5$ mN, $\rho = 1000$ kg/m^3, $v = 0.40$, $R = 0.5$ mm and $\rho_s = 9000$ kg/m^3).

The displacements of the sphere located at a viscoelastic elastic medium interface for different densities and viscosities of the medium are shown in figure 12 ($f_0 = 0.5$ mN, $E = 10000$ Pa, $v = 0.40$, $R = 0.5$ mm and $\rho_s = 9000$ kg/m^3). The spectrums of the time domain data are also included in figure 12. It is seen that, although there is no effect of the density of the medium on the steady-state displacement (being 126.7 μm for three cases here), it has a considerable effect on the amplitudes of oscillations. The effect of the density of the medium on the amplitudes of oscillations decreases as medium viscosity increases. The frequency of oscillations decreases with medium density. For example, the frequency of oscillations is 180, 177 and 172 Hz for $\rho = 1000$, 2000 and 4000 kg/m^3, respectively, when $\eta = 2$ Pa s. These results show that the density of medium needs to be taking into account for dynamic loading.

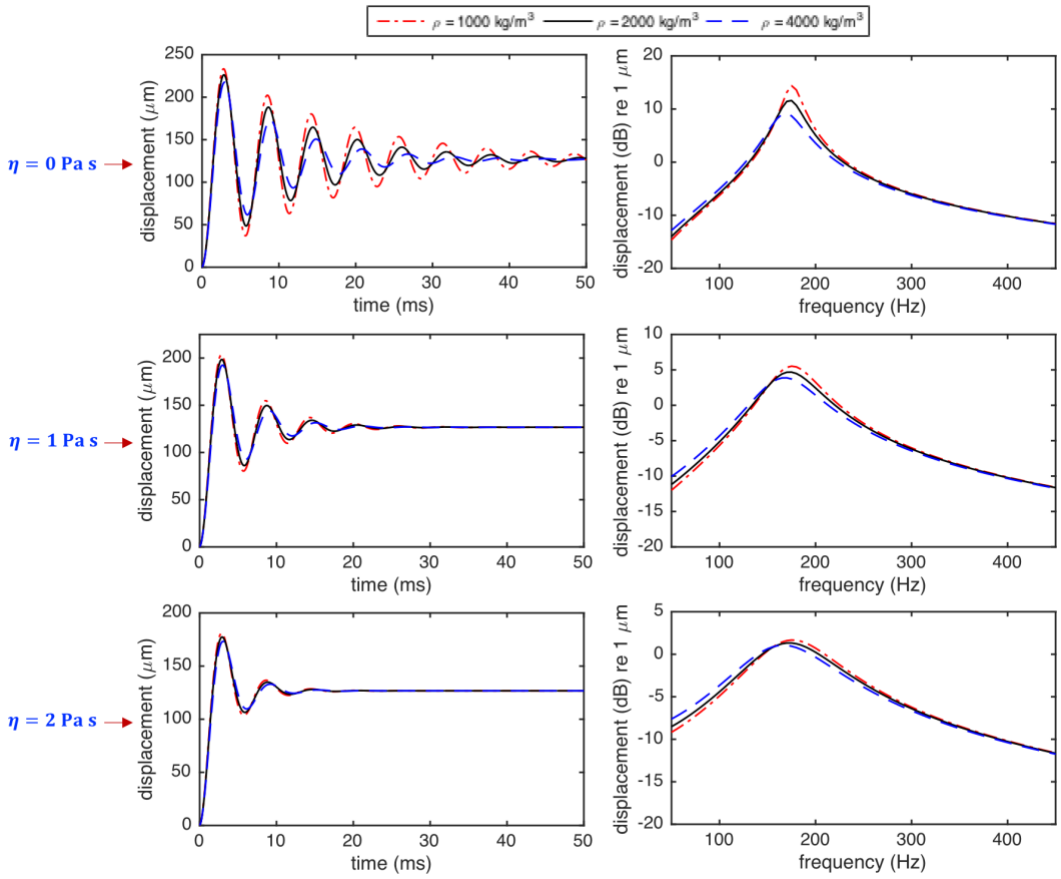

Figure 12. The displacements of the sphere located at a viscoelastic elastic medium interface for different densities and viscosities of the medium ($f_0 = 0.5$ mN, $E = 10000$ Pa, $v = 0.40$, $R = 0.5$ mm and $\rho_s = 9000$ kg/m^3).

The displacements of the sphere located at a viscoelastic medium interface for different sphere densities and medium viscosities are shown in figure 13 ($f_0 = 0.5$ mN, $E = 10000$ Pa, $v = 0.40$, $R = 0.5$ mm and $\rho = 1000$ kg/m^3). The spectrums of the time domain data are also shown in figure 13. It is seen that, although there is no effect of the density of the sphere on the steady-state displacement, its effect on the amplitudes and frequency of oscillations is significant. These results show that the density of the sphere should be taken into account for dynamic loading. It should be noted that the experimental investigation using spheres at viscoelastic medium interfaces exposed to dynamic forces will be considered in future studies.

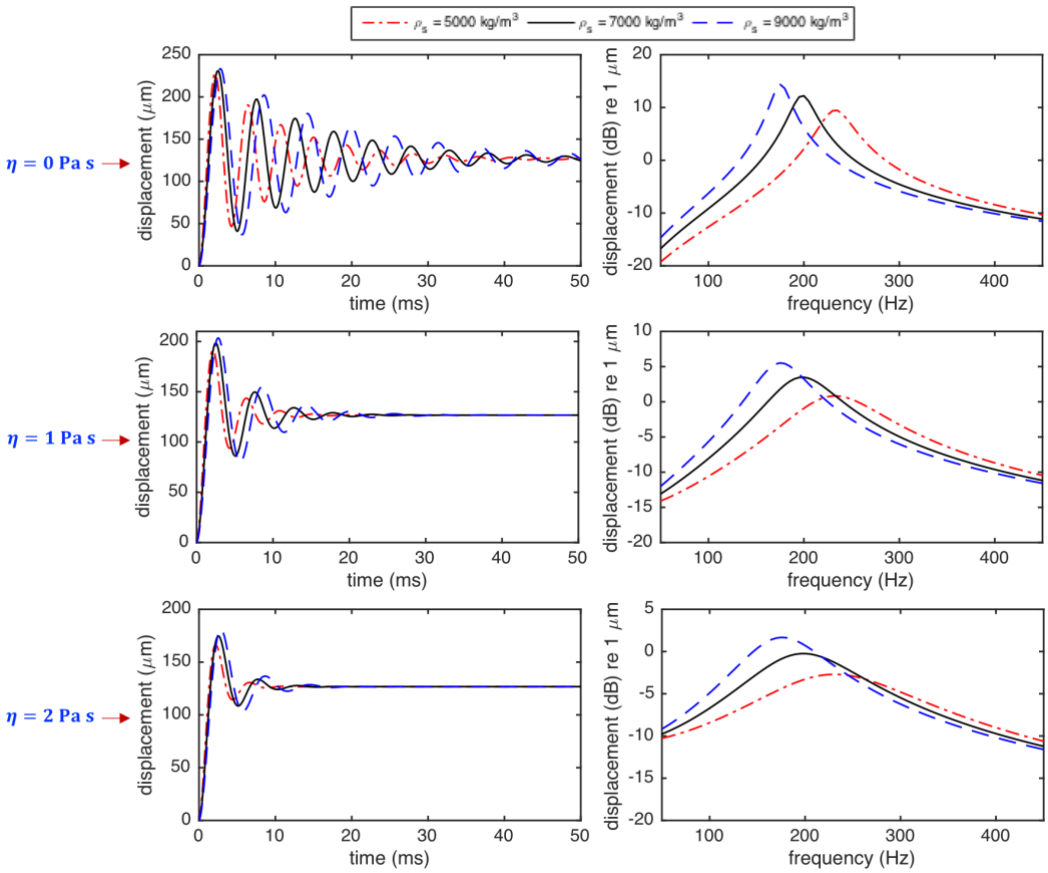

Figure 13. The displacements of the sphere located at a viscoelastic medium interface for different sphere densities and medium viscosities ($f_0 = 0.5$ mN, $E = 10000$ Pa, $v = 0.40$, $R = 0.5$ mm and $\rho = 1000$ kg/m^3).

Here, we briefly evaluate the characteristic time scales for the viscoelastic medium interacting with the sphere and wave propagation. For the Kelvin-Voigt model, the characteristic relaxation time can be simply estimated by $\overline{\tau} = \eta/G$ [43,44]. For example, for the medium with $E = 10000$ Pa or $G = 3571$ Pa, $\rho = 2000$ kg/m^3 and $\eta = 2$ Pa s in figure 12, the characteristic relaxation time can be calculated to be $\overline{\tau} = 0.56$ ms. As seen in figure 12, the characteristic time for wave propagation or the period of oscillations for the sphere ($R = 0.5$ mm and $\rho_s = 9000$ kg/m^3) located at the same medium interface is $\overline{T} = 5.65$ ms. It should be noted that the characteristic relaxation time is much less than the period of oscillations in all test cases used in this study. Furthermore, the experimental and theoretical studies performed on the dynamic responses of the spheres located inside phantoms showed that the responses predicted by the theoretical models match well with the measured responses [25,26]. The mechanical properties of the viscoelastic phantoms and the sizes of the spheres used in these studies [25,26] are similar to the ones used in this current study. For example, for the medium (gelation) properties $G = 1863$ Pa, $\rho = 1010$ kg/m^3 and $\eta = 0.61$ Pa s used in [26], the characteristic relaxation time based on the Kelvin-Voigt model can be calculated to be $\overline{\tau} = 0.33$ ms and the measured and predicted period of oscillations for the

sphere ($R = 1$ mm and $\rho_s = 7800$ kg/m^3) located inside the same medium is around $\overline{T} = 3.5$ ms [26]. These time scales are similar to the ones obtained in our study.

The model proposed in this study can be used to understand the dynamic responses of spherical objects located at viscoelastic medium interfaces in practical applications. The developed model can be used to identify both the elastic and damping properties of materials and identify the physical properties (e.g., radius and mass) of the objects at interfaces using experimental data. It is believed that the proposed model can be a significant tool for graduate students and researchers in the fields of engineering, materials science and physics to gain insight into the dynamic responses of spheres located at viscoelastic medium interfaces. Specifically, the students and researchers can clearly observe the performances of different mathematical models commonly used for predicting the static displacement of the sphere located at an elastic medium interface (Section 2). The complicated systems can be modelled using finite elements and more accurate analytical models can be obtained by exploiting the finite element analysis results (Sections 2 and 3). Using the procedure followed in this study, the students and researchers can understand, based on the need, how to convert the equation of motion in the time domain to the frequency domain, how to include the viscosity of the medium in the model and how to solve the complicated equation of motion in the frequency domain using the inverse Fourier transformation (Section 4). The procedure followed in this study can be exploited by instructors for teaching purposes.

5. Conclusion

In this study, first the mathematical models commonly used for predicting the static displacement of a sphere located at an elastic medium interface are presented and their performances are compared. After that, based on the finite element analyses, an accurate mathematical model to predict the static displacement of a sphere located at an elastic medium interface valid for different Poisson's ratios of the medium and small and large sphere displacements is proposed. Then, an improved mathematical model for the dynamic response of a sphere located at a viscoelastic medium interface is developed. In addition to the Young's modulus of the medium and the radius of the sphere, the model takes into account the density, Poisson's ratio and viscosity of the medium, the mass of the sphere and the radiation damping. The effects of the radiation damping, the Young's modulus, density and viscosity of the medium and the density of the sphere on the dynamic response of the sphere located at a viscoelastic medium interface are explored.

The results show that, for any force and Poisson's ratio, the amplitudes and period of oscillations and the steady-state displacement predicted by the model proposed in this study are very close to the ones predicted by the finite element model. The damping due to the oscillations of the sphere due to the radiation of shear waves is considerable and it should be considered for dynamic loading. The amplitudes of oscillations significantly decrease with damping as expected. The system reaches the steady-state after a while and the time to reach the steady-state decreases as the viscosity of the medium increases. The spectrums clearly show the changes in the amplitudes and frequency of oscillations. The results show that, although there is no effect of the radiation damping, the density and viscosity of the medium

and the density of sphere on the steady-state displacement, their effects on the amplitudes and frequency of oscillations are significant, hence they should be taken into account for dynamic loading.

The developed model can be used to understand the dynamic responses of spherical objects located at viscoelastic medium interfaces in practical applications. Furthermore, the proposed model is a significant tool for graduate students and researchers in the fields of engineering, materials science and physics to gain insight into the dynamic responses of spheres at viscoelastic medium interfaces. The students and researchers clearly see the performances of different mathematical models commonly used for predicting the static displacement of the sphere located at an elastic medium interface. Using the procedure presented in this study, the students and researchers can understand, based on the need, how to convert the equation of motion in the time domain to the frequency domain, how to include the viscosity of the medium in the model, and how to solve the complicated equation of motion using the inverse Fourier transform.

ORCID

Hasan Koruk: https://orcid.org/0000-0003-4189-6678

References

[1] Kontomaris S V and Stylianou A 2017 Atomic force microscopy for university students: applications in biomaterials *Eur. J. Phys.* **38** 33003

[2] Binnig G, Quate C F and Gerber C 1986 Atomic force microscope *Phys. Rev. Lett.* **56** 930–3

[3] Kontomaris S V, Stylianou A, Nikita K S and Malamou A 2019 Determination of the linear elastic regime in AFM nanoindentation experiments on cells *Mater. Res. Express* **6** 115410

[4] Chang Y-R, Raghunathan V K, Garland S P, Morgan J T, Russell P and Murphy C J 2014 Automated AFM force curve analysis for determining elastic modulus of biomaterials and biological samples. *J. Mech. Behav. Biomed. Mater.* **37** 209–18

[5] Heim A J, Matthews W G and Koob T J 2006 Determination of the elastic modulus of native collagen fibrils via radial indentation *Appl. Phys. Lett.* **89** 181902

[6] Johnson K L 1985 *Contact Mechanics* (Cambridge University Press)

[7] Kontomaris S V and Malamou A 2021 A novel approximate method to calculate the force applied on an elastic half space by a rigid sphere *Eur. J. Phys.* **42** 25010

[8] Kontomaris S V, Malamou A and Stylianou A 2020 A new approach for the AFM-based mechanical characterization of biological samples *Scanning* **2020** 2896792

[9] Wang Q J and Zhu D 2013 Hertz Theory: Contact of Spherical Surfaces *Encyclopedia of Tribology* ed Q J Wang and Y-W Chung (Boston, MA: Springer US) pp 1654–62

[10] Sneddon I N 1965 The relation between load and penetration in the axisymmetric boussinesq problem for a punch of arbitrary profile *Int. J. Eng. Sci.* **3** 47–57

[11] Guo Z, Hao M, Jiang L, Li D, Chen Y and Dong L 2020 A modified Hertz model for finite spherical indentation inspired by numerical simulations *Eur. J. Mech. - A/Solids* **83** 104042

[12] Dimitriadis E K, Horkay F, Maresca J, Kachar B and Chadwick R S 2002 Determination of elastic moduli of thin layers of soft material using the atomic force microscope *Biophys. J.* **82** 2798–810

[13] Kontomaris S-V and Malamou A 2020 Small oscillations of a rigid sphere on an

elastic half space: a theoretical analysis *Eur. J. Phys.* **41** 55004
[14] Kontomaris S-V and Malamou A 2021 Exploring the non-linear oscillation of a rigid sphere on an elastic half-space *Eur. J. Phys.* **42** 25011
[15] Koruk H 2021 Development of a model for predicting dynamic response of a sphere at viscoelastic interface: A dynamic Hertz model *IOP Conf. Ser. Mater. Sci. Eng.* **1150** 012015
[16] Aglyamov S R, Karpiouk A B, Ilinskii Y A, Zabolotskaya E A and Emelianov S Y 2007 Motion of a solid sphere in a viscoelastic medium in response to applied acoustic radiation force: Theoretical analysis and experimental verification *J. Acoust. Soc. Am.* **122** 1927–36
[17] Koruk H and Choi J J 2018 Displacement of a bubble by acoustic radiation force into a fluid-tissue interface *J. Acoust. Soc. Am.* **143** 2535–40
[18] Koruk H and Choi J J 2019 Displacement of a bubble located at a fluid-viscoelastic medium interface *J. Acoust. Soc. Am.* **145** EL410-EL416
[19] Koruk H 2021 Assessment of the models for predicting the responses of spherical objects in viscoelastic mediums and at viscoelastic interfaces *IOP Conf. Ser. Mater. Sci. Eng.* **1150** 012016
[20] Koruk H 2021 Modelling small and large displacements of a sphere on an elastic half-space exposed to a dynamic force *Eur. J. Phys.* **52** 055006
[21] Roeder R K 2013 Chapter 3 - Mechanical Characterization of Biomaterials ed A Bandyopadhyay and S B T-C of B Bose (Oxford: Academic Press) pp 49–104
[22] Dollet B, Marmottant P and Garbin V 2019 Bubble dynamics in soft and biological matter *Annu. Rev. Fluid Mech.* **51** 331–55
[23] Al-Furjan M S H, Farrokhian A, Keshtegar B, Kolahchi R and Trung N-T 2021 Dynamic stability control of viscoelastic nanocomposite piezoelectric sandwich beams resting on Kerr foundation based on exponential piezoelasticity theory *Eur. J. Mech. - A/Solids* **86** 104169
[24] Bezer J H, Koruk H, Rowlands C J and Choi J J 2020 Elastic deformation of soft tissue-mimicking materials using a single microbubble and acoustic radiation force *Ultrasound Med. Biol.* **46** 3327–38
[25] Urban M W, Nenadic I Z, Mitchell S A, Chen S and Greenleaf J F 2011 Generalized response of a sphere embedded in a viscoelastic medium excited by an ultrasonic radiation force *J. Acoust. Soc. Am.* **130** 1133–41
[26] Cebrecos A, Jiménez N, Tarazona R, Company M, Benlloch J M and Camarena F 2021 Characterization of viscoelastic media combining ultrasound and magnetic-force induced vibrations on an embedded soft magnetic sphere *IEEE Trans. Ultrason. Ferroelectr. Freq. Control* **68** 3540–8
[27] Al-furjan M S H, Farrokhian A, Keshtegar B, Kolahchi R and Trung N 2020 Higher order nonlocal viscoelastic strain gradient theory for dynamic buckling analysis of carbon nanocones *Aerosp. Sci. Technol.* **107** 106259
[28] Pouresmaeeli S, Ghavanloo E and Fazelzadeh S A 2013 Vibration analysis of viscoelastic orthotropic nanoplates resting on viscoelastic medium *Compos. Struct.* **96** 405–10
[29] Kolahchi R and Kolahdouzan F 2021 A numerical method for magneto-hygro-thermal dynamic stability analysis of defective quadrilateral graphene sheets using higher order nonlocal strain gradient theory with different movable boundary conditions *Appl. Math. Model.* **91** 458–75
[30] Taherifar R, Zareei S A, Bidgoli M R and Kolahchi R 2021 Application of differential quadrature and Newmark methods for dynamic response in pad concrete foundation covered by piezoelectric layer *J. Comput. Appl. Math.* **382** 113075

[31] Hajmohammad M H, Farrokhian A and Kolahchi R 2021 Dynamic analysis in beam element of wave-piercing Catamarans undergoing slamming load based on mathematical modelling *Ocean Eng.* **234** 109269
[32] Al-furjan M S H, Farrokhian A, Mahmoud S R and Kolahchi R 2021 Dynamic deflection and contact force histories of graphene platelets reinforced conical shell integrated with magnetostrictive layers subjected to low-velocity impact *Thin-Walled Struct.* **163** 107706
[33] Huang Y H 1967 Stresses and displacements in viscoelastic layered systems under circular loaded areas *52nd Annual Meeting of the Highway Research Board* (Washington: Highway Research Board) pp 60–71
[34] Graham G A C 1968 The correspondence principle of linear viscoelasticity theory for mixed boundary value problems involving time-dependent boundary regions *Q. Appl. Math.* **26** 167–74
[35] Khazanovich L 2008 The elastic–viscoelastic correspondence principle for non-homogeneous materials with time translation non-invariant properties *Int. J. Solids Struct.* **45** 4739–47
[36] Elisabeth A, Roman L and Christian P 2009 Multiscale prediction of viscoelastic properties of asphalt concrete *J. Mater. Civ. Eng.* **21** 771–80
[37] Lai C and Ozcebe A 2016 Causal damping ratio spectra and dispersion functions in geomaterials from the exact solution of Kramers-Kronig equations of viscoelasticity *Continuous Media with Microstructure 2* ed B Albers and M Kuczma (Springer) pp 367–82
[38] Nguyen V T and Hwu C 2020 Indentation by multiple rigid punches on two-dimensional anisotropic elastic or viscoelastic solids *Int. J. Mech. Sci.* **178** 105595
[39] Wu C-E, Lin K-H and Juang J-Y 2016 Hertzian load–displacement relation holds for spherical indentation on soft elastic solids undergoing large deformations *Tribol. Int.* **97** 71–6
[40] Puricelli L, Galluzzi M, Schulte C, Podestà A and Milani P 2015 Nanomechanical and topographical imaging of living cells by atomic force microscopy with colloidal probes *Rev. Sci. Instrum.* **86** 33705
[41] Sanliturk K Y and Koruk H 2013 Development and validation of a composite finite element with damping capability *Compos. Struct.* **97** 136–146
[42] Ilinskii Y A, Meegan G D, Zabolotskaya E A and Emelianov S Y 2005 Gas bubble and solid sphere motion in elastic media in response to acoustic radiation force *J. Acoust. Soc. Am.* **117** 2338–46
[43] Gonzalez-Gutierrez J and Scanlon M G 2018 Chapter 5 - Rheology and Mechanical Properties of Fats *Structure-Function Analysis of Edible Fats* ed A G Marangoni (AOCS Press) pp 119–68
[44] Araújo G R d. S, Viana N B, Gómez F, Pontes B and Frases S 2019 The mechanical properties of microbial surfaces and biofilms *Cell Surf.* **5** 100028